

# Augmented Neural Ordinary Differential Equations for Power System Identification

Hannes M. H. Wolf\* Christian A. Hans\*

\* *Automation and Sensorics in Networked Systems, University of Kassel, Germany (e-mail: {h.wolf, hans}@uni-kassel.de)*

**Abstract:** Due the complexity of modern power systems, modeling based on first-order principles becomes increasingly difficult. As an alternative, dynamical models for simulation and control design can be obtained by black-box identification techniques. One such technique for the identification of continuous-time systems are neural ordinary differential equations. For training and inference, they require initial values of system states, such as phase angles and frequencies. While frequencies can typically be measured, phase angle measurements are usually not available. To tackle this problem, we propose a novel structure based on augmented neural ordinary differential equations, learning latent phase angle representations on historic observations with temporal convolutional networks. Our approach combines state-of-the art deep learning techniques, avoiding the necessity of phase angle information for the power system identification. Results show, that our approach clearly outperforms simpler augmentation techniques.

**Keywords:** Machine and deep learning for system identification, Nonlinear system identification

## 1. INTRODUCTION

In power systems engineering, dynamical models are crucial for simulation, analysis and control design. Traditionally, such models are obtained using first order principles. In future power systems with a large number of distributed renewable and storage units, this approach is becoming increasingly difficult. At the same time, ongoing digitalization and widespread deployment of sensors in powergrids offer a vast amount of measurements that open the door for data-driven system identification. Here, dynamical models are obtained even without knowledge of the underlying processes, which can be particularly useful for large scale future power systems.

A modern technique for black-box system identification are neural ordinary differential equations (ODEs). They were first introduced by Chen et al. (2018) and allow to represent the right hand side of an ODE as a neural network (NN). Since then, several extensions to neural ODEs (NODEs) have been proposed. Massaroli et al. (2020) introduced data-controlled NODEs which allow to incorporate external control and disturbance inputs. Furthermore, Dupont et al. (2019) introduced augmented NODEs that enable latent representations of unmeasured states. In the power system domain, several studies have employed NODEs to identify components or entire power systems. Aryal et al. (2023) employed NODEs to identify linearized input/output (I/O) frequency dynamics of droop-controlled synchronous generators (SGs). However, coupling between SGs was not considered. Zhang et al. (2024) used NODEs to identify the frequency dynamics of the entire IEEE 118 bus system. They focused on generator angle and frequency trajectories under fault scenarios. Wolf and Hans (2025) considered coupled dynamics of droop-controlled grid-forming inverters (GFIs).

Using desired frequency and voltage setpoints as control input, voltage and frequency dynamics were identified with NODEs and compared to symbolic regression. All of the aforementioned studies assumed that phase angles and frequency of all units are available. Opposed to this, Xiao et al. (2023) used NODEs to identify the dynamics of power system components from portal measurements. They emphasize scenarios where the system state could not be measured and employ autoencoders to obtain initial states from available values of a single time instant.

Typically, observations of a single time instant do not suffice to uniquely determine a system state. This is why Masti and Bemporad (2018), as well as Forgione et al. (2022) use a time series of historic observations of system inputs and outputs to learn the initial state for neural state space models using deep autoencoders and long short-term memorys (LSTMs), respectively. In this paper we build on this idea and extend it for augmented NODEs in order to learn latent representations for non-measured system states, i.e., unknown phase angles. Our contributions are as follows: 1) We combine state-of-the-art deep learning frameworks for system identification. In detail, we propose a novel structure that, for the first time, employs temporal convolutional networks (TCNs) to augment unmeasured states in NODEs. 2) We learn voltage and frequency dynamics of entire power systems with our novel structure, without using phase angle information. This is crucial, as phase angle measurements can only be obtained with costly measurement equipment, such as phasor measurement units. 3) We conduct large scale hyperparameter optimizations to learn models for three power systems of different size. In a numerical case study, we show that our approach outperforms augmented NODEs with simpler augmentation techniques.

The paper is structured as follows. In Section 2, we define our notation and introduce fundamental NN structures. Section 3 discusses power system models. In Section 4, we describe the fundamentals of NODEs, bridge the gap from machine learning (ML) to system identification and introduce our novel approach. The case study and the results are presented in Section 5. Section 6 concludes the paper.

## 2. PRELIMINARIES

### 2.1 Notation

We denote the set of real numbers by  $\mathbb{R}$ , the set of non-negative real numbers by  $\mathbb{R}_{\geq 0}$ , the set of strictly positive real numbers by  $\mathbb{R}_{>0}$ , the set of nonnegative integers  $\mathbb{N}$  and the set of complex numbers by  $\mathbb{C}$ . An element  $z \in \mathbb{C}$  is  $z = a + ib$  where  $i$  is the imaginary unit,  $a \in \mathbb{R}$  is the real part and  $b \in \mathbb{R}$  is the imaginary part. We denote datasets as  $\mathcal{D} = \{(\xi_n, \eta_n)\}_{n=1}^N$  where the  $n$ -th sample  $(\xi_n, \eta_n)$  consists of features  $\xi_n \in \mathbb{R}^{n_\xi}$ , i.e., the inputs to a ML model, and targets  $\eta_n \in \mathbb{R}^{n_\eta}$ , i.e., the expected outputs for features  $\xi_n$ .

### 2.2 Neural networks

*Multilayer perceptrons* A multilayer perceptron (MLP) is a feedforward NN with  $n_\xi \in \mathbb{N}$  inputs and  $n_\eta \in \mathbb{N}$  outputs consisting of  $L \in \mathbb{N}$  fully connected layers of neurons. Each layer  $l \in \{1, \dots, L\}$  contains  $N_{f,l}$  neurons and applies an affine transformation, which is, except for the last layer, followed by a nonlinear activation function  $\sigma$ . The input  $\xi \in \mathbb{R}^{n_\xi}$  is mapped to the output with

$$f_\theta(\xi) = W_L \sigma(W_{L-1} \dots \sigma(W_1 \xi + b_1) \dots + b_{L-1}) + b_L, \quad (1)$$

where  $W_i \in \mathbb{R}^{N_{f,i} \times N_{f,i-1}}$  are weights and  $b_i \in \mathbb{R}^{N_{f,i}}$  are biases, i.e., the parameters  $\theta$  of the NN, with  $N_{f,0} = n_\xi$  and  $N_{f,L} = n_\eta$ .

*Temporal convolutional networks* TCNs (Bai et al., 2018) are based on causal convolutions, which allow to capture temporal dependencies in sequences. Consider the sequence  $\xi = \{\xi(t_1), \xi(t_2), \dots, \xi(t_T)\}$  of length  $T$  with  $\xi(t_k) \in \mathbb{R}^I$ , where  $I \in \mathbb{N}$  is the number of channels. When using the entire sequence as an input to a causal 1D-convolutional layer, we obtain a sequence  $\eta$  at the output of same length but with  $O \in \mathbb{N}$  channels, i.e.,  $\eta(t_k) \in \mathbb{R}^O$ . At channel  $o \in [1, O] \subset \mathbb{N}$  the output at time  $t_k$  is

$$\eta_o(t_k) = b^o + \sum_{i=1}^I \sum_{j=0}^{K-1} W_{i,j}^o \xi_i(t_{k-dj}) \quad (2)$$

with kernel  $W^o \in \mathbb{R}^{K \times I}$  and bias  $b^o \in \mathbb{R}$ . The dilation  $d \in \mathbb{N}$  is the temporal spacing between elements of the inputs in the convolution.

We use residual blocks  $h_b$ ,  $b \in [0, B-1] \subset \mathbb{N}$  as described in Bai et al. (2018), where one residual block consists of two convolutional layers (2), each with  $O_b$  hidden channels followed by a rectified linear unit (ReLU). The output sequence of such a residual connection for input  $\xi$  is

$$\eta = \xi + h_b(\xi). \quad (3)$$

Finally, TCNs consist of  $B$  consecutive residual connections with an exponentially growing dilation  $d_b = 2^b$ . Thus,

there are  $\sum_{l=0}^{B-1} 2O_b$  kernels and biases, which are the parameters of the TCN. The effective history of the TCN is

$$R = 1 + 2(K-1)(2^B - 1), \quad (4)$$

i.e., in order to utilize all  $\xi(t_k)$  of input  $\xi$  for  $\eta(t_T)$  of output  $\eta$ ,  $R \geq T$  must hold.

## 3. MODELING

In what follows, we derive the mathematical model of the power system components. We assume balanced three-phase grids and represent electrical quantities using complex numbers in a rotating coordinate system. The network, as well as the dynamic models of the units mainly follow Schiffer (2015).

### 3.1 Network model

The electrical network is modelled as a graph  $\mathcal{G} = (\mathcal{N}, \mathcal{E}, y)$ , where  $\mathcal{N}$  is the set of  $|\mathcal{N}|$  nodes,  $\mathcal{E} \subseteq \mathcal{N} \times \mathcal{N}$  the set of edges and  $y : \mathcal{E} \rightarrow \mathbb{C}$ ,  $y((i, j)) = y_{ij} = g_{ij} + ib_{ij}$  is a weighting function returning the admittance of the edge  $(i, j)$ . Here  $g_{ij} \in \mathbb{R}_{\geq 0}$  and  $b_{ij} \in \mathbb{R}$  denote the conductance and the susceptance, respectively. In this context, self edges  $(i, i) \in \mathcal{E}$  are associated with parallel shunt admittances to the ground and  $(i, j) \in \mathcal{E}$ ,  $i \neq j$  with series admittances between distinct nodes. The set of nodes adjacent to  $i \in \mathcal{N}$  is referred to as  $\mathcal{N}_i \subset \mathcal{N}$ . Each node  $i \in \mathcal{N}$  is associated with a voltage phasor  $\tilde{v}_i = v_i e^{i\varphi_i} \in \mathbb{C}$ , where  $v_i \in \mathbb{R}_{\geq 0}$  is the voltage amplitude and  $\varphi_i \in \mathbb{R}$  the voltage phase angle. Furthermore, each node is equipped with a local  $dq$ -coordinate system rotating with  $\omega_i \in \mathbb{R}$ , whose  $q$ -axis is aligned with the voltage phasor. We express phase angle differences of these coordinate systems to a global reference  $dq$ -system as  $\delta_i = \varphi_i - \varphi_{\text{ref}}$ , and thus  $\dot{\delta}_i = \omega_i - \omega_{\text{ref}}$ .

Consider the admittance matrix  $Y \in \mathbb{C}^{|\mathcal{N}| \times |\mathcal{N}|}$  (Kundur et al., 1994) constructed from  $y_{ij}, \forall (i, j) \in \mathcal{E}$ , as well as the vectors  $\tilde{v} \in \mathbb{C}^{|\mathcal{N}|}$  and  $c \in \mathbb{C}^{|\mathcal{N}|}$  collecting the node voltages and injected currents of each node, respectively. We can compute the injected complex power for all nodes with  $s = \tilde{v}c^* = \tilde{v}(Y\tilde{v})^*$ . Using  $s_i = p_i + iq_i$ , where  $p_i \in \mathbb{R}$  is the active and  $q_i \in \mathbb{R}$  the reactive power, as well as  $\delta_{ij} = \delta_i - \delta_j$ , we obtain

$$\begin{aligned} p_i &= v_i^2 g_{ii} + v_i \sum_{j \in \mathcal{N}_i} v_i g_{ij} - v_j (g_{ij} \cos(\delta_{ij}) + b_{ij} \sin(\delta_{ij})), \\ q_i &= -v_i^2 b_{ii} - v_i \sum_{j \in \mathcal{N}_i} v_i b_{ij} + v_j (g_{ij} \sin(\delta_{ij}) - b_{ij} \cos(\delta_{ij})). \end{aligned} \quad (5)$$

### 3.2 Unit models

We consider setups, where each node  $i \in \mathcal{N}$  is equipped with a droop-controlled GFI or a SG. The set of nodes with GFIs is denoted by  $\mathcal{N}_{\text{gfi}}$  and the set of nodes with SGs by  $\mathcal{N}_{\text{sg}}$ . We proceed to derive state models for both of them.

*Remark 1.* In future power systems, GFIs are taking over parts of the ancillary services that are provided by SGs in traditional power systems. They can, e.g., operate together with a storage unit providing positive or negative active power to the grid.

*Remark 2.* It is possible to consider power systems containing a set of passive nodes  $\mathcal{N}_{\text{pas}}$  that do not have a GFI or an SG connected, i.e.,  $\mathcal{N} = \mathcal{N}_{\text{gfi}} \cup \mathcal{N}_{\text{sg}} \cup \mathcal{N}_{\text{pas}}$ . Such systems can also be modelled using our methods by transforming them into the presented ones by applying Kron reduction (Dörfler and Bullo, 2013). This maintains the dynamical behavior and thus the resulting state trajectories at nodes  $i \in \mathcal{N}_{\text{gfi}} \cup \mathcal{N}_{\text{sg}}$ . In practice, system identification would be performed on data obtained from nodes  $i \in \mathcal{N}_{\text{gfi}} \cup \mathcal{N}_{\text{sg}}$  without requiring a Kron-reduction step beforehand.

*Grid-forming inverters* Droop-controlled GFIs change frequency and voltage amplitude according to deviations in active and reactive power. Following standard practice, we assume these adjustments take place instantaneously (Schiffer et al., 2014), i.e.,

$$\omega_i = \omega_i^d - k_i^p(p_i^m - p_i^d), \quad (6a)$$

$$v_i = v_i^d - k_i^q(q_i^m - q_i^d). \quad (6b)$$

where  $p_i^d, q_i^d \in \mathbb{R}$  denote the active and reactive power setpoint, respectively. Moreover,  $\omega_i^d, v_i^d \in \mathbb{R}_{>0}$  are the frequency and voltage amplitude setpoint, respectively, and  $k_i^p, k_i^q \in \mathbb{R}_{>0}$  are droop gains. We assume that active and reactive power measurements,  $p_i^m$  and  $q_i^m \in \mathbb{R}$ , are processed using a first-order low-pass filter with time constant  $\tau_i \in \mathbb{R}_{>0}$  (Schiffer et al., 2014), i.e.,

$$\tau_i \dot{p}_i^m = -p_i^m + p_i, \quad (7a)$$

$$\tau_i \dot{q}_i^m = -q_i^m + q_i. \quad (7b)$$

Combining (6) and (7) yields the GFIs' state model at node  $i$ , i.e.,

$$\dot{\delta}_i = \omega_i^d - k_i^p(p_i^m - p_i^d) - \omega_{\text{ref}}, \quad (8a)$$

$$\dot{p}_i^m = \frac{1}{\tau_i}(-p_i^m + p_i), \quad (8b)$$

$$\dot{v}_i = \frac{1}{\tau_i}(-v_i + v_i^d - k_i^q(q_i^m - q_i^d)). \quad (8c)$$

*Synchronous generators* The frequency dynamics of SGs are modelled using the swing equation (Schiffer, 2015), i.e.,

$$m_i \dot{\omega}_i = -k_i^d(\omega_i - \omega_d) + p_i^m - p_i, \quad (9)$$

where  $m_i \in \mathbb{R}_{>0}$  is the inertia constant,  $k_i^d \in \mathbb{R}_{>0}$  the damping coefficient and  $p_i^m \in \mathbb{R}_{>0}$  is the mechanical power. Droop-controlled SGs change the mechanical power depending on frequency deviations (Schiffer, 2015), i.e.,

$$p_i^m = p_i^d - \frac{1}{k_i^p}(\omega_i - \omega^d). \quad (10)$$

We assume that this change in mechanical power takes place instantaneously with no delay of the governor. Additionally, we consider a similar voltage droop law as for the GFIs. To that end, we assume that the automatic voltage regulator is fast and its dynamics can be neglected such that we can set the voltage at the terminals directly. Combining (6b), (7b), (9) and (10), we obtain the SGs' state model at node  $i$ , i.e.,

$$\dot{\delta}_i = \omega_i - \omega_{\text{ref}}, \quad (11a)$$

$$\dot{\omega}_i = \frac{1}{m_i} \left( -\frac{1}{k_i^p}(\omega_i - \omega^d) + p_i^d - p_i \right), \quad (11b)$$

$$\dot{v}_i = \frac{1}{\tau_i}(-v_i + v_i^d - k_i^q(q_i^m - q_i^d)). \quad (11c)$$

Note that damping terms have already been included in the droop gain  $k_i^p$  (Schiffer, 2015).

Combining (5), (8) and (11) for all nodes in the grid allows us to derive the overall state model

$$\dot{x}(t) = f(t, x(t), u(t)) \quad (12a)$$

$$y(t) = g(x(t)) \quad (12b)$$

with state  $x(t) \in \mathbb{R}^{n_x}$ ,  $n_x = 3|\mathcal{N}|$  at time  $t$ , control input  $u(t) \in \mathbb{R}^{n_u}$ ,  $n_u = |\mathcal{N}|$  and output  $y(t) \in \mathbb{R}^{n_y}$ ,  $n_y = 2|\mathcal{N}|$ . Here,  $x$  contains the states, i.e.,  $\delta_i(t), p_i^m(t), v_i(t)$  for GFIs and  $\delta_i(t), \omega_i(t), v_i(t)$  for SGs, of all units  $i \in \mathcal{N}$ . As control inputs we choose the active power setpoints, i.e.,  $u(t) = [p_1^d(t) \ \dots \ p_N^d(t)]^T$ . The states  $v_i(t), \omega_i(t)$ ,  $\forall i \in \mathcal{N}_{\text{sg}}$  and  $v_i(t), p_i^m(t)$ ,  $\forall i \in \mathcal{N}_{\text{gfi}}$  are outputs, i.e.,  $\delta_i(t)$ ,  $\forall i \in \mathcal{N}$  is not available to the outside.

## 4. NEURAL ORDINARY DIFFERENTIAL EQUATIONS

Since a large number of systems can be modeled in the form of (12), NODEs are a natural choice for black-box system identification. Generally speaking, our goal is to approximate the I/O behaviour of (12) with NODEs.

NODEs (Chen et al., 2018) represent ODEs where the right hand side is a NN  $f_{\theta_f}$  with parameters  $\theta_f \in \mathbb{R}^{n_{\theta_f}}$ , i.e.,

$$\dot{x}(t) = f_{\theta_f}(t, x(t)), \quad x(t_s) = x_0 \quad (13)$$

Given the initial state  $x_0$  at time  $t_s$ , we can use a numerical solver to find a solution to the initial value problem (IVP) associated with (13) at time  $t_e > t_s$ . Here,  $x_0$  is contained in the features  $\xi$ , i.e., the inputs to the ML model.

To represent (12), we use the more general NODE model formulated by Massaroli et al. (2020), i.e.,

$$\dot{x}(t) = f_{\theta_f}(t, x(t), e_{\theta_e}(\xi)), \quad (14a)$$

$$x(t_s) = h_{\theta_h}(\xi), \quad (14b)$$

$$y(t) = g(x(t)). \quad (14c)$$

Here, the solution to the IVP is

$$\hat{y}(t) = g_{\theta_g}(h_{\theta_h}(\xi) + \int_{t_s}^{t_e} f_{\theta_f}(t, x(t), e_{\theta_e}(\xi)) dt). \quad (15)$$

Model (14) extends (13) by three concepts. The first one is called augmentation and was first introduced by Dupont et al. (2019). In augmented neural ordinary differential equations (A-NODEs),  $\xi$  is elevated into a higher dimensional space to increase the NODEs' expressiveness. Possible augmentation techniques are zero-augmentation  $x(t_s) = [\xi^T \ 0^T]^T$  (Dupont et al., 2019), input-layer augmentation  $x(t_s) = h_{\theta_h}(\xi)$  or partial input-layer augmentation  $x(t_s) = [\xi^T \ h_{\theta_h}^T(\xi)]^T$  (Massaroli et al., 2020). The second concept is called data-controlled neural ordinary differential equations (D-NODEs), and was first introduced by Massaroli et al. (2020). Here, the right hand side is conditioned on  $\xi$ . This can be done in an explicit or an implicit fashion. For the latter, an additional embedding function  $e_{\theta_e}$  is employed. Lastly, a function  $g_{\theta_g}$  is employed to map the state space to the output space.

From a control perspective, these extensions come naturally. However, the terminology is often different:  $\xi$  typically contains known control inputs  $u$ , as well as past and present measurements of  $y$ , but often no entire state

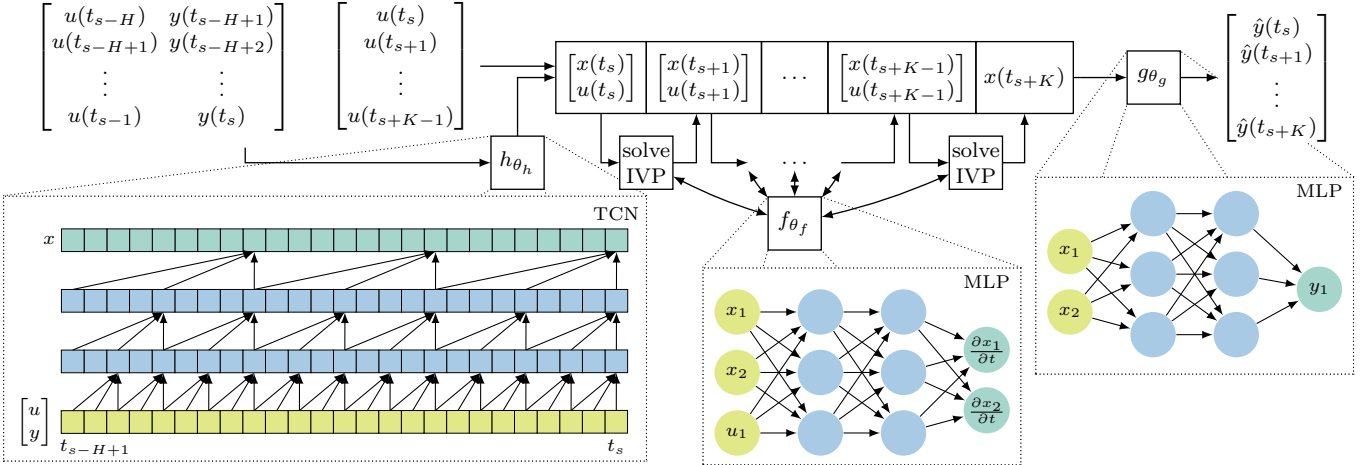


Fig. 1. ML model for system identification. Note that all depictions of the NNs are simplified. For the TCN, e.g., we omit the residual blocks and show only convolutional layers instead.

measurements. Augmentation means finding  $x_0$  from information contained in  $\xi$ . Furthermore, D-NODEs allow us to incorporate constant control inputs. Then,  $e_{\theta_e}(\xi) = u(t_s)$  is just an extraction of  $u(t_s)$  from  $\xi$  rather than an embedding.

We aim to approximate (12) with (14). In what follows, we discuss different parts of the ML model which is shown in Figure 1. First, we describe how to obtain an initial state from a sequence of past observations with a TCN  $h_{\theta_h}$  in Section 4.1. In Section 4.2, we define the MLPs  $f_{\theta_f}$  and  $g_{\theta_g}$  used to model the dynamics. Sections 4.3 and 4.4 discuss how to step the model forward in time and train it, respectively. We start with some assumptions.

*Assumption 1.* We restrict ourselves to time-invariant systems and drop the argument  $t$  in  $f_{\theta_f}$ .

*Assumption 2.* All quantities are sampled at discrete time instants  $t_0, t_1, \dots, t_s, \dots, t_T$  with constant sampling time  $\Delta t = t_{s+1} - t_s$ .

*Assumption 3.* The control input  $u(t)$  is piecewise constant over each sampling interval, i.e.,  $u(t) = u(t_s)$  for all  $t \in [t_s, t_{s+1})$ .

#### 4.1 Obtaining an initial state with $h_{\theta_h}$

For system identification, augmentation is crucial since the dimension of the output space is typically smaller than the dimension of the state space. Rahman et al. (2022) propose input-layer augmentation with  $x(t_s) = h_{\theta_h}(u(t_s), y(t_s))$ . In practice  $x(t_s)$  can usually not be uniquely determined from  $u(t_s)$  and  $y(t_s)$  at a single time instant. However, under certain conditions this is possible when  $H \geq n_x$  past observations are used (Forgione et al., 2022). Therefore, we learn a latent representation  $x(t_s)$  of the actual system state from a history of  $H$  observations instead. To the best of our knowledge, for the first time TCNs (see Section 2.2.2) are employed for this task in this paper.

The methodology is sketched in the lower left corner of Figure 1. Each  $u_i$  and each  $y_i$  corresponds to an input channel of the TCN. With the convolution (2) and ReLU activations they are mapped to hidden channels in the residual blocks. Eventually, after the last residual block we obtain a sequence for  $x(t_{s-H+1}), \dots, x(t_s)$  and extract

$x(t_s)$ . The number of residual blocks  $B$  is chosen such that  $R \geq H$ , where  $R$  is obtained according to (4). We abuse the notation of the argument of  $h_{\theta_h}$  to match the interface of the TCN and write

$$h_{\theta_h}(\xi) = h_{\theta_h} \left( \begin{bmatrix} u(t_{s-H}) & \dots & u(t_{s-1}) \\ y(t_{s-H+1}) & \dots & y(t_s) \end{bmatrix} \right). \quad (16)$$

*Remark 3.* If the output can be partitioned such that  $y(t) = [x^o(t) \ \tilde{y}(t)]^T$  where  $x^o$  the part of  $x$  that is directly available and  $\tilde{y}$  are the remaining outputs, we can also opt for a partial augmentation  $x(t_s) = [x^o(t_s) \ h_{\theta_h}^T(\xi)]^T$ .

#### 4.2 Modeling the dynamics with $f_{\theta_f}$ and $g_{\theta_g}$

Let us now discuss  $f_{\theta_f}$  and  $g_{\theta_g}$  that approximate the I/O dynamics. We use D-NODEs as described beforehand and condition  $f_{\theta_f}$  on the control inputs. Thus, we model  $f_{\theta_f}$  as a NN with inputs  $u(t_s)$  and  $x(t)$ , as well as outputs  $\dot{x}(t)$  using an MLP (see Section 2.2.1). Similarly, we can use an MLP  $g_{\theta_g}$  for the output mapping. Figure 1 sketches their use in the ML model. Combining aforementioned concepts and assuming constant control inputs over  $[t_s, t_e]$ , the model reads

$$\dot{x}(t) = f_{\theta_f}(x(t), u(t_s)), \quad (17a)$$

$$x(t_s) = h_{\theta_h} \left( \begin{bmatrix} u(t_{s-H}) & \dots & u(t_{s-1}) \\ y(t_{s-H+1}) & \dots & y(t_s) \end{bmatrix} \right) \quad (17b)$$

$$\hat{y}(t) = g_{\theta_g}(x(t)). \quad (17c)$$

For the power system problem at hand, we assume that  $y$  is a measured part of the system state  $x$ , i.e.,  $g_{\theta_g}(x) = x^o$ . Accordingly, we preserve the physical meaning of the measured states in the NODE by choosing a partial augmentation of the initial state and obtain

$$\dot{x}(t) = f_{\theta_f}(t, x(t), u(t_s)), \quad (18a)$$

$$x(t_s) = \left[ h_{\theta_h} \left( \begin{bmatrix} u(t_{s-H}) & \dots & u(t_{s-1}) \\ x^o(t_{s-H+1}) & \dots & x^o(t_s) \end{bmatrix} \right) \right], \quad (18b)$$

$$\hat{y}(t) = x^o(t). \quad (18c)$$

### 4.3 Moving the model forward in time

In closed-loop simulations,  $u(t)$  typically varies over time. Thus, an IVP with initial time  $t_s$  might also contain stepwise changes in  $u$  over the time horizon  $[t_s, t_e]$ .

Considering  $t_s, t_{s+1}, \dots, t_{s+K} \in [t_s, t_e]$ , where  $K$  is the prediction horizon, we proceed as depicted in Figure 1. For given  $H$  past measurements of  $u$  and  $y$ , we augment the system state at time  $t_s$  using  $h_{\theta_h}$  and solve the IVP up to time  $t_{s+1}$  in order to obtain  $x(t_{s+1})$ . For the subsequent time intervals  $[t_{s+k}, t_{s+k+1}]$ ,  $k = 1, \dots, k = K - 1$ , we do not need augmentation. Instead, we can use the solution  $x(t_{s+k})$  as the initial state for the IVPs and condition  $f_{\theta_f}$  on  $u(t_{s+k})$ . Thereby, we repeatedly solve an IVP to step the model forward in time and obtain predictions  $\hat{y}(t_{s+1}), \dots, \hat{y}(t_{s+K})$ .

### 4.4 Training the model

We train the model on the dataset  $\mathcal{D} = \{(\xi_n, \eta_n)\}_{n=1}^N$ . From the different parts explained in Sections 4.1–4.3, we end up with features and targets of the form

$$\begin{aligned}\xi_n &= [u^T(t_{s_n-H}) \dots u^T(t_{s_n+K}) \ y^T(t_{s_n-H+1}) \dots y^T(t_{s_n})]^T, \\ \eta_n &= [y^T(t_{s_n+1}) \dots y^T(t_{s_n+K})]^T,\end{aligned}$$

and minimize the mean square error between the targets  $\eta_n$  and the predictions resulting from  $\xi_n$ , i.e.,

$$L = \frac{1}{NK} \sum_{n=1}^N \sum_{k=1}^K \|y(t_{s_n+k}) - \hat{y}_n(t_{s_n+k})\|_2^2. \quad (19)$$

To obtain  $\partial L / \partial \theta$ , we use the "discretize-then-optimize" approach (Kidger, 2022), propagating gradients through solver operations.

## 5. CASE STUDY

In what follows, we employ the methods from Section 4 to identify systems of the form described in Section 3. In particular, we consider three grids of different size: the IEEE 9 bus system (IEEE9), the IEEE 30 bus system (IEEE30) and the IEEE 39 bus system (IEEE39). The systems' information were retrieved from Matpower (Zimmerman et al., 2011). We collected line admittance data, as well as passive loads derived from demand data. For nodes equipped with units, we used the generation data as nominal active and reactive power setpoints  $p^d$  and  $q^d$ . We considered unit models (8) and (11) according to Table 1. Thus, we obtain diverse setups: an SG dominated IEEE9, a GFI dominated IEEE30 and the IEEE39 with SGs only. The global coordinate system is set to be equal to the local  $dq$ -coordinate system of the reference node according to Table 1. The parameters, i.e., droop gains, time constants and inertia constants are varied arbitrarily around typical values.

Table 1. Generators of the test systems.

System	$\mathcal{N}_{\text{gfi}}$	$\mathcal{N}_{\text{sg}}$	node for $\omega_{\text{ref}}, \varphi_{\text{ref}}$
IEEE9	{1}	{2, 3}	1
IEEE30	{1, 22, 23, 27}	{2, 13}	1
IEEE39	{}	{30, 31, ..., 39}	31

Recall from Section 3 that the voltage amplitude  $v_i$  at all nodes, as well as the frequency  $\omega_i$  at SG nodes and the power  $p_i^m$  at GFI nodes are measured. Measurements of voltage phase angles  $\delta_i$  at the nodes were not available at all. The numerical integration method used with NODEs is fourth-order Runge-Kutta (RK4) with a fixed step-size equal to sampling step-size. We made use of the torchdiffeq package by Chen (2018) which implements differentiable solvers in pytorch. For adjusting the weights of the models, we used the Adam optimizer (Kingma and Ba, 2017).

### 5.1 Setup

**Data generation** The data was obtained from numerical simulations. For each system, we simulated three trajectories of length 250s for training, validation and testing, as well as one trajectory of length 1010s for evaluation, at a sampling frequency of 100 Hz each. As control inputs, we used random step changes in active power setpoints  $p_i^d$ , distributed equally within  $\pm 0.2$  pu around their nominal values. In the trajectories of length 250s, they occur every 5s, in the trajectories of length 1010s every 10s. We simulated that each available output is affected by zero-mean Gaussian noise, such that each normalized signal has a signal to noise ratio of 25 dB.

**Remark 4.** Typically, a tertiary controller would change the setpoints on a timescale of several minutes. Such dynamic responses could realistically be captured over multiple setpoint changes, irrespective of their actual occurrence by selecting appropriate observation windows.

**Samples and datasets** Based on the previously generated data, we formed four distinct datasets: For each system, we created one training, one validation, one testing and one evaluation dataset. The training dataset  $\mathcal{D}^1$  was used to adjust the parameters  $\theta$  of the model. The validation dataset  $\mathcal{D}^2$  was used to monitor the training progress, i.e., to stop the training and to choose the best model over the epochs. For hyperparameter optimization, we relied on the error on the test dataset  $\mathcal{D}^3$ . Finally, the evaluation dataset  $\mathcal{D}^4$  was used to assess the performance of the selected model.

To create the datasets  $\mathcal{D}^m = \{(\xi_n, \eta_n)\}_{n=1}^{N_m}$ ,  $m \in [1, 4] \subset \mathbb{N}$ ,  $N_m \in \mathbb{N}$ , we constructed samples from simulated trajectories. We adopted the methodology presented in Forgione and Piga (2021) and cut out  $N_m$  subsequences of length  $H + K + 1$  from  $t_{s_n-H}$  to  $t_{s_n+K}$  with a temporal distance  $D$ . Figure 2 illustrates this procedure. For  $\mathcal{D}^1$ ,  $\mathcal{D}^2$  and

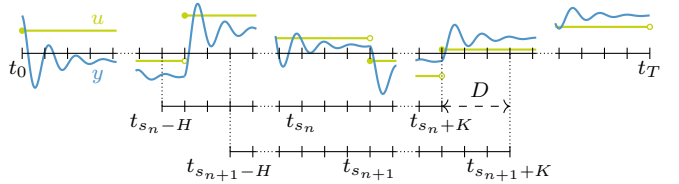


Fig. 2. Cutting out two consecutive subsequences  $n$  and  $n + 1$  with  $D = 3$  from a trajectory. Illustration inspired by Forgione and Piga (2021).

$\mathcal{D}^3$  we chose  $H = 64$  historic time instants, a prediction horizon of  $K = 64$  instants and  $D = 16$ . For each, we

cut out subsequences for  $s_n = H + (n - 1)D$  from the trajectories of length 250s and formed samples  $(\xi_n, \eta_n)$  as described in Section 4.4. We collected these samples into batches of size 256 for training. To create  $\mathcal{D}^4$ , we used the trajectory of length 1010s and chose  $H = 64$ ,  $K = 500$  as well as  $D = 1000$ . Subsequences were cut out for  $s_n = 1000 + (n - 1)D$  such that for each resulting sample,  $t_{s_n}$  aligns with the step changes in the control inputs at  $t_{\text{step}_n} = 10\text{s}, 20\text{s}, \dots, 1000\text{s}$ . Thus, we used 100 samples in total for the evaluation.

*Hyperparameter Optimization* As hyperparameters, we considered the network sizes, i.e., the number of layers  $L_f$  and hidden units  $N_f$  of the MLP representing  $f_{\theta_f}$ , as well as the number of hidden channels  $N_h$  used for the TCN  $h_{\theta_h}$ . Note that we chose the minimum number of residual blocks  $B$  such that  $R \geq H$  and thus did not optimize the depth of the TCN. Table 2 summarizes the search space. For Bayesian optimization of the hyperparameters, we used a sampler based on the tree-structured Parzen estimator (Bergstra et al., 2011) and a 25%-percentile pruner employing optuna (Akiba et al., 2019).

Table 2. Hyperparameter search space.

Hyperparameter	Intervals/sets
$f_{\theta_f}$ hidden layers	$L_f \in \{2^k \mid k = 0, 1, 2\} \subset \mathbb{N}_{\geq 0}$
$f_{\theta_f}$ hidden neurons/layer	$N_f \in \{2^k \mid k = 5, 6, \dots, 10\} \subset \mathbb{N}_{\geq 0}$
$h_{\theta_h}$ hidden channels	$N_h \in \{2^k \mid k = 5, 6, \dots, 10\} \subset \mathbb{N}_{\geq 0}$
Learning rate	$\alpha \in [10^{-4}, 10^{-2}] \subset \mathbb{R}_{\geq 0}$
$f_{\theta_f}$ activation function	$\sigma(\cdot) \in \{\text{Softplus}, \text{GELU}, \text{SiLU}\}$

## 5.2 Results

In what follows, we analyze hyperparameter choice and prediction accuracy. We refer to our models as TCN-A-NODE. As a baseline, we use model (18) replacing (18b) with simple partial input-layer augmentation that does not consider historic data, i.e.,  $x(t_s) = [x^o(t_s) \ h_{\theta_h}^T(x^o(t_s))]^T$ , where  $h_{\theta_h}$  is an MLP. A comparable approach has been used by Xiao et al. (2023). We refer to these models as MLP-A-NODE. We always use the best model found in the hyperparameter optimization for each power system and each augmentation method. We analyze the predictions of voltage magnitudes and frequencies on a previously unseen dataset. Note that  $w_i$  was obtained using (6a) for all  $i \in \mathcal{N}_{\text{gfi}}$ .

*Hyperparameter Choice* Table 3 shows the the best hyperparameters found for each system for the TCN-A-NODE. In general, we observe that for  $f_{\theta_f}$  shallow networks with only one hidden layer perform best. Considering the number of hidden neurons per layer of  $f_{\theta_f}$ , the results vary between the systems. For the IEEE9 less hidden neurons than for the IEEE30 and the IEEE39 were required to capture the dynamics accurately. The same holds for the number of hidden channels of the TCN  $h_{\theta_h}$ . However, we would like to emphasize, that for all systems, the error barely changed when double or half the number of hidden neurons or channels were chosen. The learning rate was found to be in typical ranges for NN training, but it was necessary to adjust it accordingly for the respective network size. From all the smooth activation functions, we

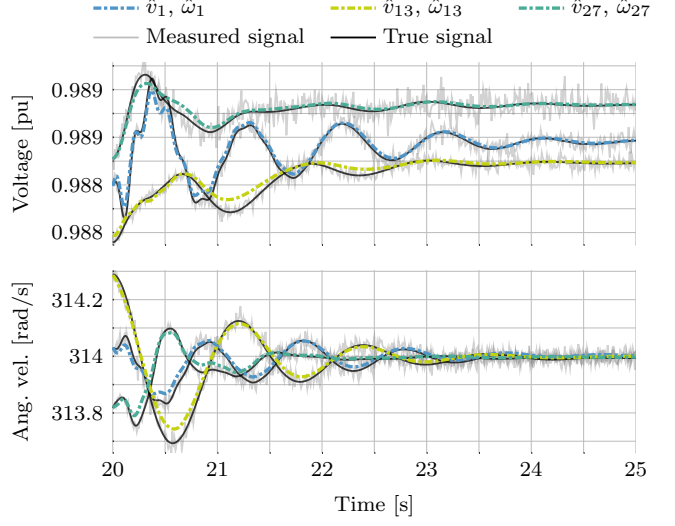


Fig. 3. Voltage amplitude and frequency responses for the IEEE30 at nodes 1,13 and 27 to a step change in  $p_i^d$  for all units at  $t_s = 20\text{s}$ .

found that the sigmoid linear unit (SiLU) performed best across all systems.

Table 3. Best Hyperparameters for all systems with the TCN-A-NODE.

System	IEEE9	IEEE30	IEEE39
$f_{\theta_f}$ hidden layers	1	1	1
$f_{\theta_f}$ hidden neurons	128	1024	512
$h_{\theta_h}$ hidden channels	32	64	64
Learning rate	$5.22 \cdot 10^{-3}$	$4.43 \cdot 10^{-3}$	$1.01 \cdot 10^{-3}$
$f_{\theta_f}$ activation fct.	SiLU	SiLU	SiLU

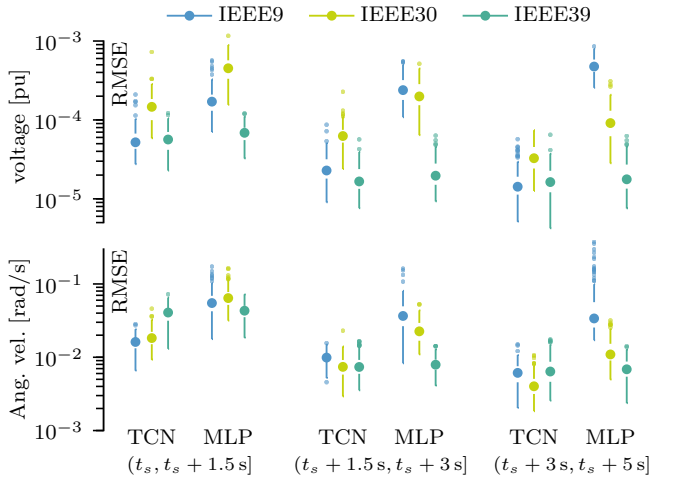


Fig. 4. Box plots of the prediction RMSE of 100 step responses for all systems over a horizon of 5s splitted into different time intervals.

*Prediction Accuracy* To analyze the prediction accuracy of the learned models we use the evaluation dataset  $\mathcal{D}^4$ . For all units, each sample is associated with a prediction of  $\omega_i$  and  $v_i$  to a step change in  $p_i^d$  at time  $t_{s_n}$ . Figure 3 shows an example trajectory of such a response for the IEEE30 at nodes 1, 13 and 27 for sample  $n = 2$ . A visual

inspection indicates that frequency and voltage dynamics are captured well by the learned model. Transient errors at the beginning of the response are small, emphasizing the quality of the learned initial state. Figure 4 visualizes the model accuracy in a quantitative manner using the root-mean-square-error (RMSE) associated with all 100 samples. The RMSE is calculated for three time intervals  $(t_s, t_s + 1.5 \text{ s}]$ ,  $(t_s + 1.5 \text{ s}, t_s + 3 \text{ s}]$  and  $(t_s + 3 \text{ s}, t_s + 5 \text{ s}]$  capturing short-term, medium-term and long-term accuracy, respectively, ranging from highly dynamic to quasi steady-state conditions.

Our novel TCN-A-NODE reaches strong steady state accuracy. The slightly decreased short-term accuracy most likely originates from small errors in the augmented part of  $x(t_s)$  as well as noise in  $x^o(t_s)$  which directly translates into errors in initial state  $x(t_s)$ . However, these errors fade over time as the system converges to steady state. Meanwhile, the MLP-A-NODE shows significantly larger errors in all time brackets and fails to capture the dynamics accurately for the IEEE9 and IEEE30 test cases. A visual inspection of the MLP-A-NODE trajectories of the IEEE9 test case showed that the resulting trajectories drifted, eventually leading to instability over a longer time horizon. This shows that the TCN-A-NODE allows learn appropriate latent representation of phase angles resulting in an overall accurate identification, while the MLP-A-NODE fails to achieve this goal.

## 6. CONCLUSION

In this paper, we proposed a novel structure based on A-NODEs to identify power system dynamics. We employed a TCN to learn latent representations for phase angles based on historic observations. The approach allows for accurate identification without the necessity of phase angle measurements and outperforms simpler augmentation techniques, that are widely employed. In the future, we intend to combine known and unknown parts for the system identification, as well as architectural novelties like graph NODEs to identify power system dynamics.

## REFERENCES

Akiba, T., Sano, S., Yanase, T., Ohta, T., and Koyama, M. (2019). Optuna: A next-generation hyperparameter optimization framework. In *ACM SIGKDD Int. Conf. Knowl. Discov. Data Min.*, 2623–2631.

Aryal, T., Aslami, P., Bhujel, N., Rekabdarkolaei, H.M., Fu, K., and Hansen, T.M. (2023). Application of neural ordinary differential equations to power system frequency dynamics. In *NAPS*, 1–6.

Bai, S., Kolter, J.Z., and Koltun, V. (2018). An empirical evaluation of generic convolutional and recurrent networks for sequence modeling. URL <https://arxiv.org/abs/1803.01271>.

Bergstra, J., Bardenet, R., Bengio, Y., and Kégl, B. (2011). Algorithms for hyper-parameter optimization. In *NeurIPS*, volume 24.

Chen, R.T.Q. (2018). `torchdiffeq`. URL <https://github.com/rtqichen/torchdiffeq>.

Chen, R.T.Q., Rubanova, Y., Bettencourt, J., and Duvenaud, D.K. (2018). Neural Ordinary Differential Equations. In *NeurIPS*, volume 31.

Dörfler, F. and Bullo, F. (2013). Kron Reduction of Graphs With Applications to Electrical Networks. *IEEE Trans. Circuits Syst. I Regul. Pap.*, 60(1), 150–163.

Dupont, E., Doucet, A., and Teh, Y.W. (2019). Augmented Neural ODEs. In *NeurIPS*, volume 32.

Forgione, M., Mejari, M., and Piga, D. (2022). Learning neural state-space models: do we need a state estimator? URL <https://arxiv.org/abs/2206.12928>.

Forgione, M. and Piga, D. (2021). Continuous-time system identification with neural networks: Model structures and fitting criteria. *Eur. J. Control*, 59, 69–81.

Kidger, P. (2022). *On Neural Differential Equations*. Phd thesis, University of Oxford. URL <https://arxiv.org/abs/2202.02435>.

Kingma, D.P. and Ba, J. (2017). Adam: A Method for Stochastic Optimization. URL <https://arxiv.org/abs/1412.6980>.

Kundur, P., Balu, N.J., and Lauby, M.G. (1994). *Power system stability and control*. The EPRI power system engineering series. McGraw-Hill, New York, USA.

Massaroli, S., Poli, M., Park, J., Yamashita, A., and Asama, H. (2020). Dissecting Neural ODEs. In *NeurIPS*, volume 33, 3952–3963.

Masti, D. and Bemporad, A. (2018). Learning nonlinear state-space models using deep autoencoders. In *57th IEEE CDC*, 3862–3867.

Rahman, A., Dragoña, J., Tuor, A., and Strube, J. (2022). Neural ordinary differential equations for nonlinear system identification. In *ACC*, 3979–3984.

Schiffer, J. (2015). *Stability and power sharing in microgrids*. Phd thesis, Technische Universität Berlin.

Schiffer, J., Ortega, R., Astolfi, A., Raisch, J., and Sezi, T. (2014). Conditions for stability of droop-controlled inverter-based microgrids. *Automatica*, 50(10), 2457–2469.

Wolf, H.M.H. and Hans, C.A. (2025). Identification of power systems with droop-controlled units using neural ordinary differential equations. In *ECC*, 800–806.

Xiao, T., Chen, Y., Huang, S., He, T., and Guan, H. (2023). Feasibility Study of Neural ODE and DAE Modules for Power System Dynamic Component Modeling. *IEEE Trans. Power Syst.*, 38(3), 2666–2678.

Zhang, S., Yamashita, K., and Yu, N. (2024). Learning Power System Dynamics with Noisy Data Using Neural Ordinary Differential Equations. In *IEEE PESGM*, 1–5.

Zimmerman, R.D., Murillo-Sánchez, C.E., and Thomas, R.J. (2011). Matpower: Steady-state operations, planning, and analysis tools for power systems research and education. *IEEE Trans. Power Syst.*, 26(1), 12–19.